ATLAS NOTE

ATLAS-CONF-2012-076

August 12, 2012

Search for direct slepton and gaugino production in final states with two leptons and missing transverse momentum with the ATLAS detector in pp collisions at $\sqrt{s} = 7$ TeV

The ATLAS Collaboration

Abstract

A search for the electroweak pair production of charged sleptons and weak gauginos decaying into final states with two leptons is performed using 4.7 fb^{-1} of proton-proton collision data at $\sqrt{s} = 7$ TeV recorded with the ATLAS experiment at the Large Hadron Collider. No significant excesses are observed with respect to the prediction from Standard Model processes. In the scenario of direct slepton production, if the sleptons decay directly into the lightest neutralino, left-handed slepton masses between 90 and 185 GeV are excluded at 95% confidence level for a 20 GeV neutralino. Chargino masses between 110 and 330 GeV are excluded in the scenario of direct production of wino-like chargino pairs decaying into the lightest neutralino via an intermediate on-shell charged slepton for a 10 GeV neutralino.

This note was revised on the 12th August to fix errors in Figure 4. In the previous version of this note Figures 4 (b)-(c) were not correctly truncated at 40 GeV, and Figure 4 (d) displayed the diboson component as evaluated with Sherpa, not Herwig. Additionally, a plotting error had resulted in a missing uncertainty band on the last bin of each histogram.

1 Introduction

Weak scale Supersymmetry (SUSY) [1–9] is an extension to the Standard Model (SM). It postulates for each known boson or fermion the existence of a particle whose spin differs by one-half unit from the SM partner. The introduction of these new particles provides solutions to the hierarchy problem [10–13] and, if R-parity is conserved [14–18], a dark matter candidate in the form of the lightest supersymmetric particle (LSP). R-parity conservation is assumed in this paper, hence SUSY particles are always produced in pairs. In a large fraction of the SUSY parameter space the LSP is the weakly interacting lightest neutralino, $\tilde{\chi}_1^0$.

Gluinos ($\tilde{g}$) and squarks ($\tilde{q}$) are the SUSY partners of gluons and quarks. Charginos ($\tilde{\chi}_i^{\pm}$, $i = 1, 2$) and neutralinos ($\tilde{\chi}_j^0$, $j = 1, 2, 3, 4$) are the mass eigenstates formed from the linear superposition of the SUSY partners of the Higgs and electroweak gauge bosons: higgsinos, winos and the bino (collectively, gauginos). Sleptons ($\tilde{l}^{\pm}$) are the SUSY partners of the charged leptons: selectron, smuon and stau. If the masses of the gluinos and squarks are greater than a few TeV and the weak gauginos and sleptons have masses of a few hundreds of GeV, the direct production of weak gauginos and sleptons may dominate the production of SUSY particles at the Large Hadron Collider (LHC). Such a scenario is possible in the general framework of the phenomenological minimal supersymmetric SM (pMSSM) [19]. Naturalness suggests that third generation sparticles, charginos and neutralinos should have masses of a few hundreds of GeV [20]. Light sleptons are expected in Gauge Mediated [21] and Anomaly Mediated [22] SUSY breaking scenarios. Light sleptons could also play a role in helping SUSY to provide a relic dark matter density consistent with observations [23].

This note presents the first search for direct slepton pair production at the LHC and a dedicated search for direct chargino pair production in final states with two leptons (electrons, e or muons, μ).

1.1 Direct Slepton and Chargino Pair Production

Sleptons can be produced directly in a process similar to Drell-Yan production [24]. The search in this note targets the direct pair production of left-handed charged sleptons, where each charged slepton $\tilde{l}$ (selectron or smuon) decays through $\tilde{l}^{\pm} \rightarrow l^{\pm}\tilde{\chi}_1^0$, yielding a final state with two same flavour (SF) charged leptons. The undetected $\tilde{\chi}_1^0$ gives rise to large missing transverse momentum in the event. Previous experimental searches for direct slepton production [25] assumed gaugino unification. In the present work this assumption is dropped, thereby removing the lower limit on the mass of the $\tilde{\chi}_1^0$. Direct chargino pair production, where each chargino decays through $\tilde{\chi}_1^{\pm} \rightarrow l^{\pm}\nu\tilde{\chi}_1^0$ leads to a signature similar to that of slepton pair production. The search in this note targets this production channel and subsequent decay, setting limits on the chargino mass, without the assumptions on the mass of the $\tilde{\chi}_2^0$ usually present in tri-lepton searches.

1.2 Other Weak Gaugino Production

In the general framework of the pMSSM, several weak gaugino production channels can lead to final states with two leptons. Production modes such as $\tilde{\chi}_2^0\tilde{\chi}_{i=1,2}^{\pm}$ or $\tilde{\chi}_2^0\tilde{\chi}_{j=2,3,4}^0$, with the subsequent decays $\tilde{\chi}_2^0 \rightarrow l^{\pm}l^{\mp}\tilde{\chi}_1^0$ and $\tilde{\chi}_j^0, \tilde{\chi}_i^{\pm} \rightarrow q\bar{q}'\tilde{\chi}_1^0$ are addressed by a signal region containing two leptons and two jets. In order to complement existing and future tri-lepton searches a dedicated signal region with two same charge leptons is designed to be sensitive to trilepton final states from $\tilde{\chi}_2^0\tilde{\chi}_1^{\pm} \rightarrow (l^{\pm}l^{\mp}\tilde{\chi}_1^0) + (l^{\pm}\nu\tilde{\chi}_1^0)$ where one lepton is not identified. All final states yield missing transverse energy due to the presence of two $\tilde{\chi}_1^0$'s.

Model-independent visible cross-section upper limits are set in each signal region to address the large variety of possible production and decay modes in the gaugino sector. This search is not sensitive to weak

gaugino decays via on-shell Z-bosons. Previous limits on weak chargino and neutralino production have been placed at LEP [25], the Tevatron [26, 27] and at the LHC [28–30].

2 The ATLAS Detector

The ATLAS experiment [31] is a multi-purpose particle physics detector with a forward-backward symmetric cylindrical geometry and nearly 4π coverage in solid angle.[1] It contains four superconducting magnet systems, which include a thin solenoid surrounding the inner tracking detector (ID), and barrel and endcap toroids supporting a muon spectrometer. The ID consists of a silicon pixel detector, a silicon microstrip detector (SCT), and a transition radiation tracker (TRT). In the pseudorapidity region $|\eta| < 3.2$, high-granularity liquid-argon (LAr) electromagnetic (EM) sampling calorimeters are used. An iron-scintillator tile calorimeter provides coverage for hadron detection over $|\eta| < 1.7$. The end-cap and forward regions, spanning $1.5 < |\eta| < 4.9$, are instrumented with LAr calorimeters for both EM and hadronic measurements. The muon spectrometer surrounds the calorimeters and consists of a system of precision tracking chambers ($|\eta| < 2.7$), and detectors for triggering ($|\eta| < 2.4$).

3 Monte Carlo

3.1 Standard Model Production

Monte Carlo (MC) simulated event samples are used to develop and validate the analysis procedure and to evaluate the SM backgrounds in the signal region. The dominant backgrounds include fully-leptonic $t\bar{t}$, Z/γ^*+jets, single top and dibosons (WW, WZ and ZZ). Production of top quark pairs is simulated with `POWHEG` [32], using a top quark mass of 172.5 GeV. Samples of W to $l\nu$ and Z/γ^* to ll, produced with accompanying jets (of both light and heavy flavour), are obtained with `ALPGEN` [33]. Diboson (WW, WZ, ZZ) production is simulated with `SHERPA` [34] in signal regions requiring jets and with `HERWIG` [35] elsewhere. Single top production is modelled with `MC@NLO`. Fragmentation and hadronisation for the `ALPGEN` and `MC@NLO` samples are performed with `HERWIG`, using `JIMMY` [36] for the underlying event, and with `PYTHIA` for the `POWHEG` sample. Expected diboson yields are normalised using NLO QCD predictions obtained with `MCFM` [37, 38]. The top-quark contribution is normalised to approximate next-to-next-to-leading order (NNLO) calculations [39]. The inclusive W and $Z/\gamma*$ production cross-sections are normalised to the next-to-next-to-leading order (NNLO) cross-sections obtained using `FEWZ` [40]. `MC@NLO` [41] samples are used to assess the systematic uncertainties associated with the choice of generator for $t\bar{t}$ production, and `AcerMC` [42] samples are used to assess the uncertainties associated with initial and final state radiation (ISR/FSR) [43]. `ALPGEN`, `HERWIG` and `SHERPA` samples are used to assess the systematics associated with the choice of generator for diboson production.

3.2 Direct Slepton and Direct Gaugino Production

Four signal regions are designed in this paper, optimised for the discovery of various SUSY models which directly produce sleptons and gauginos. SUSY signal samples are generated in the pMSSM framework at fixed slepton and neutralino masses, and at fixed gaugino mass parameters. The former is used to set limits on the masses of the sleptons in direct slepton pair production, whereas the latter is used to design an analysis sensitive to the variety of direct gaugino production modes already described. Samples are also produced in a simplified model at fixed LSP and chargino masses, which are then used to set limits

[1] ATLAS uses a right-handed coordinate system with its origin at the nominal interaction point in the centre of the detector and the z-axis along the beam pipe. Cylindrical coordinates (r, ϕ) are used in the transverse plane, ϕ being the azimuthal angle around the beam pipe. The pseudorapidity η is defined in terms of the polar angle θ by $\eta = -\ln\tan(\theta/2)$.

on the chargino mass, independent of the $\tilde{\chi}_2^0$ mass. In all SUSY models the masses of the squarks, gluinos and third generation supersymmetric partners of the fermions are large (2.5 TeV in the direct slepton production pMSSM models and 2 TeV in the direct gaugino pMSSM and simplified models).

The direct slepton models are based on those which are described in Ref. [44]. Masses of all gauginos apart from the $\tilde{\chi}_1^0$ are set to 2.5 TeV. The sensitivity of the present search to a given model is determined by the slepton production cross-section and by the mass of the $\tilde{\chi}_1^0$ which affects the kinematics of the final state leptons. The mass of the bino-like $\tilde{\chi}_1^0$ is varied by scanning values of gaugino mass parameter M_1 in steps of 20 GeV in the range 20-160 GeV. The common selectron and smuon mass is generated in the range 70-190 GeV, scanned in steps of 20 GeV with the constraint $m_{\tilde{l}} > m_{\tilde{\chi}_1^0} + 30$ GeV. The cross-section for direct slepton pair production in these models decreases from 3.9 to 0.05 pb independently of neutralino mass as the slepton mass increases from 70 to 190 GeV.

There are four parameters in the simplified models of direct gaugino production: the masses of $\tilde{\chi}_1^0$, $\tilde{\nu}$, $\tilde{\ell}_L$ and the common mass of $\tilde{\chi}_1^\pm$ and $\tilde{\chi}_2^0$. The latter are wino-like and $\tilde{\chi}_1^0$ is bino-like. The $\tilde{\chi}_1^\pm$ are pair-produced via the s-channel exchange of a virtual gauge boson and decay via left-handed sleptons, including $\tilde{\tau}$, and $\tilde{\nu}$ of mass $m_{\tilde{\nu}} = m_{\tilde{\ell}_L} = (m_{\tilde{\chi}_1^0} + m_{\tilde{\chi}_1^\pm})/2$ with a branching ratio of 50% each. The cross section for $\tilde{\chi}_1^\pm\tilde{\chi}_1^\mp$ pair production in these models is ~ 0.2 pb for $\tilde{\chi}_1^\pm$ masses between 200 and 250 GeV. For lower chargino masses ($50 - 125$ GeV) the cross-section is as high as 3 pb, dropping below 0.2 pb for models with chargino masses of 250 GeV and above.

For the other weak gaugino production channels, a set of pMSSM models with intermediate sleptons in the gaugino decay chain are generated. The right-handed sleptons, with a common mass for all three generations, are inserted half way between the two lightest neutralino masses while left-handed slepton masses are kept beyond reach. The gaugino mass parameters M_1, M_2 and μ are varied independently, the ratio of the expectation values of the two Higgs doublets ($\tan\beta$) is set to 6. In the pMSSM model the cross sections vary significantly (between 0.5 and 100 pb for $M_1 = 250$, with the highest cross-sections at low M_2 and μ). The present direct gaugino production search is only sensitive to models with intermediate sleptons.

Signal samples for the pMSSM and slepton model points are generated with `HERWIG`, whereas `Herwig++` [45] is used to generate the simplified model points. Signal cross sections are calculated to next-to-leading order in the strong coupling constant (NLO) using `PROSPINO2` [46]. The nominal cross section and the uncertainty are taken from an envelope of cross section predictions using different PDF sets and factorisation and renormalisation scales, as described in Ref. [47].

All MC samples are produced using a `GEANT4` [48] based detector simulation [49]. The effect of multiple proton-proton collisions from the same or different bunch crossings is incorporated into the simulation by overlaying additional minimum bias events onto hard scatter events using `PYTHIA`. Simulated events are weighted to match the distribution of the mean number of interactions per bunch crossing observed in data.

4 Data and Event Selection

The 7 TeV proton-proton collision data analysed were recorded between March and October 2011. Application of beam, detector and data-quality requirements yields a total integrated luminosity of 4.7 fb^{-1}. Events are triggered using a combination of single and double lepton triggers. The single electron triggers vary with the data taking period, and the tightest trigger has an efficiency of ~97% for electrons with $p_{\mathrm{T}} > 25$ GeV. The single muon trigger used for all data taking periods reaches an efficiency plateau of ~75% (~90%) in the barrel (end-caps) for muons with $p_{\mathrm{T}} > 20$ GeV. All quoted efficiencies have been measured with respect to reconstructed leptons. The double lepton triggers reach similar plateau efficiencies, but at lower p_{T} thresholds: > 17 GeV for the dielectron trigger, and > 12 GeV for the

dimuon trigger; for the electron-muon trigger the thresholds are 15 and 10 GeV respectively. One or two signal leptons are required to have triggered the event, and be matched to the online triggered leptons: one lepton, if one is above the appropriate single lepton trigger plateau threshold or two leptons, if there is no such lepton. If one lepton is below the threshold of the double lepton triggers, and the other not above the single lepton threshold, the event is rejected. An exception to this rule is applied in the $\mu\mu$ channel. In this case when one lepton has $p_{\mathrm{T}} > 20$ GeV and the second $p_{\mathrm{T}} > 12$ GeV, a logical OR of both triggers is used to recover efficiency.

Jet candidates are reconstructed using the anti-k_t jet clustering algorithm [50] with a distance parameter of 0.4. The jet candidates are corrected for the effects of calorimeter non-compensation and inhomogeneities by using p_{T} and η-dependent calibration factors based on MC simulations and validated with extensive test-beam and collision-data studies [51]. Only jet candidates with transverse momenta $p_{\mathrm{T}} > 20$ GeV and $|\eta| < 4.5$ are subsequently retained. Jets likely to have arisen from detector noise or cosmic rays are rejected [51]. Electron candidates are required to have $p_{\mathrm{T}} > 10$ GeV, $|\eta| < 2.47$, and pass the "medium" shower shape and track selection criteria of Ref. [52]. Muon candidates are reconstructed using either a full muon spectrometer track matched to an ID track, or a muon spectrometer track matched to an extrapolated ID track. They are then required to have $p_{\mathrm{T}} > 10$ GeV and $|\eta| < 2.4$. They must be reconstructed with sufficient hits in the pixel, SCT and TRT detectors.

The measurement of the missing transverse momentum two-vector, $\mathbf{p}_{\mathrm{T}}^{\mathrm{miss}}$, and its magnitude, $E_{\mathrm{T}}^{\mathrm{miss}}$, is based on the transverse momenta of all electron and muon candidates, all jets, and all calorimeter clusters with $|\eta| < 4.9$ not associated to such objects. The quantity $E_{\mathrm{T}}^{\mathrm{miss,rel.}}$ is defined as:

$$E_{\mathrm{T}}^{\mathrm{miss,rel.}} = \begin{cases} E_{\mathrm{T}}^{\mathrm{miss}} & \text{if } \Delta\phi_{\ell,j} \geq \pi/2 \\ E_{\mathrm{T}}^{\mathrm{miss}} \times \sin\Delta\phi_{\ell,j} & \text{if } \Delta\phi_{\ell,j} < \pi/2 \end{cases}, \tag{1}$$

where $\Delta\phi_{\ell,j}$ is the azimuthal angle between the direction of $\mathbf{p}_{\mathrm{T}}^{\mathrm{miss}}$ and that of the nearest electron, muon or jet. In a situation where one of the jets' or the leptons' momentum is badly reconstructed, such that it is aligned with the direction of $\mathbf{p}_{\mathrm{T}}^{\mathrm{miss}}$, only the $E_{\mathrm{T}}^{\mathrm{miss}}$ component perpendicular to that object is considered. This is used to significantly reduce mis-measured $E_{\mathrm{T}}^{\mathrm{miss}}$ in processes such as $Z/\gamma^* \rightarrow e^+e^-, \mu^+\mu^-$ [53].

Signal electrons, muons and jets are then selected. Signal electrons are further required to pass the "tight" [52] quality criteria, which places additional requirements on the ratio of calorimetric energy to track momentum, and the number of high-threshold hits in the TRT. They are also required to be isolated: the p_{T} sum of tracks above 1 GeV within a cone of size $\Delta R = \sqrt{(\Delta\eta)^2 + (\Delta\phi)^2} < 0.2$ around each electron candidate (excluding the electron candidate itself) is required to be less than 10% of the electron p_{T}. Signal muons must also be isolated: the p_{T} sum of tracks within a cone of size $\Delta R < 0.2$ around the muon candidate is required to be less than 1.8 GeV.

Signal jets are subject to the further requirements $p_{\mathrm{T}} > 30$ GeV, $|\eta| < 2.5$ and the "jet vertex fraction" [54] is reasonably high (0.75). The jet vertex fraction quantifies the fraction of track transverse momentum from the primary vertex, associated to a jet. This variable is used to remove jets that originated from other collisions, and also discards jets without reconstructed tracks.

A b-tagging algorithm [55], which exploits the long lifetime of weak b- and c-hadron decays inside a candidate jet, is used to identify jets containing a b-hadron decay. The mean nominal b-tagging efficiency, computed on $t\bar{t}$ MC events, is 80%, with a misidentification (mis-tag) rate for light-quark/gluon jets of less than 1%. Scale factors (which are p_{T} and η dependent) are applied to all MC samples to correct for small discrepancies in the b-tagging performance observed in data with respect to simulation.

Basic data quality requirements are then applied. Selected events in each signal region (SR) and control region (CR) must satisfy the following requirements. The primary vertex in the event must have at least five associated tracks and each event must contain exactly two leptons of opposite sign (OS) or same sign (SS). Both of these leptons must additionally satisfy the full list of lepton requirements, and

Targeted Process	Signal Region
Two Lepton Final States	
$\tilde{l}^{\pm}\tilde{l}^{\mp} \rightarrow (l^{\pm}\tilde{\chi}_1^0) + (l^{\mp}\tilde{\chi}_1^0)$	SR-m_{T2}
$\tilde{\chi}_1^{\pm}\tilde{\chi}_1^{\mp} \rightarrow (l^{\pm}\nu\tilde{\chi}_1^0) + (l^{\mp}\nu\tilde{\chi}_1^0)$	SR-m_{T2}, SR-OSjveto
$\tilde{\chi}_2^0\tilde{\chi}_i \rightarrow (l^{\pm}l^{\mp}\tilde{\chi}_1^0) + (q\bar{q}^{'}\tilde{\chi}_1^0)$	SR-2jets
Three Lepton Final States	
$\tilde{\chi}_2^0\tilde{\chi}_1^{\pm} \rightarrow (l^{\pm}l^{\mp}\tilde{\chi}_1^0) + (l^{\pm}\nu\tilde{\chi}_1^0)$	SR-OSjveto, SR-SSjveto

Table 1: Decay modes targeted by each SR, $\tilde{\chi}_i$ denotes either a chargino or a neutralino. In decays producing three real leptons, one must be mis-reconstructed or fall outside the acceptance of the detector.

the dilepton invariant mass, m_{ll}, must be greater than 20 GeV across all flavour combinations.

5 Signal Regions

In this analysis four SR are defined. The first and main SR (labelled SR-m_{T2}) exploits the stransverse mass variable, m_{T2} [56, 57], and provides sensitivity to both $\tilde{\chi}_1^{\pm}$ and $\tilde{l}^{\pm}$ pair production. The search for $\tilde{l}^{\pm}$ pair production uses only the same flavour channels e^+e^- and $\mu^+\mu^-$, while the $\tilde{\chi}_1^{\pm}$ pair production search also relies on $e^{\pm}\mu^{\mp}$. Additional sensitivity to $\tilde{\chi}_1^{\pm}$ pair production is provided by the next SR, SR-OSjveto, which selects OS lepton pairs with high $E_{\mathrm{T}}^{\mathrm{miss}}$ in events with no signal jets.

The production modes $\tilde{\chi}_2^0\tilde{\chi}_i^{\pm}$ or $\tilde{\chi}_2^0\tilde{\chi}_i^0$, with the subsequent decays $\tilde{\chi}_2^0 \rightarrow l^{\pm}l^{\mp}\tilde{\chi}_1^0$ and $\tilde{\chi}_i^0$,$\tilde{\chi}_i^{\pm} \rightarrow q\bar{q}'\tilde{\chi}_1^0$ are targeted by a region called SR-2jets, which selects events with two signal jets and two OS leptons.

In this note the region SR-OSjveto and an equivalent region, SR-SSjveto, which instead selects the events with SS lepton pairs, also target a three lepton final state. The explicit veto in this analysis on a third lepton makes the results in these regions orthogonal to results from direct gaugino searches with three or more leptons [29]. These regions recover events not reconstructed in a search with ≥ 3 leptons because one of the leptons falls outside the acceptance of the detector and selection criteria. The processes directly targeted by each SR are stated explicitly in Table 1.

The exact requirements on the values to be taken by each variable in each SR were determined by optimising the expected reach using the Z_n variable [58], a measure of significance, in either the neutralino-slepton mass plane of the pMSSM model (SR-m_{T2}), the neutralino-chargino mass plane of the simplified model (SR-OSjveto and SR-SSjveto) or the $M_1 - \mu$ mass plane of the pMSSM (SR-2jets). Table 2 summarises the requirements for entering each SR.

5.1 Direct Slepton and Chargino Pair Production

In SR-m_{T2} the properties of m_{T2} are exploited to search for $\tilde{l}^{\pm}\tilde{l}^{\mp}$ and $\tilde{\chi}_1^{\pm}\tilde{\chi}_1^{\mp}$ production followed by decay to final states containing exactly two OS leptons (of different flavour, DF, or same flavour, SF), no signal jets, and $E_{\mathrm{T}}^{\mathrm{miss}}$ from the two $\tilde{\chi}_1^0$. In this SR $t\bar{t}$ and WW are dominant backgrounds. For large mass differences between the sleptons (charginos) and the lightest neutralino, the m_{T2} distribution for signal events extends significantly beyond the distributions for $t\bar{t}$ and diboson backgrounds.

The optimised value for the lower m_{T2} requirement is 90 GeV, just above the W-mass (which is the approximate end-point of the WW and $t\bar{t}$ distributions). A rejection of events with m_{ll} within 10 GeV of the Z-mass reduces Z/γ^* backgrounds. For the direct slepton pMSSM models with a 20 GeV neutralino, the product of the kinematic and geometrical acceptance and reconstruction and event selection efficiencies varies between 0.1 and 4.0% in this SR for slepton masses between 90 and 190 GeV. For

SR-	m_{T2}	OSjveto	SSjveto	2jets
charge	OS	OS	SS	OS
flavour	any	any		SF
m_{ll}	Z-veto	Z-veto	-	Z-veto
signal jets	= 0	= 0		≥ 2
signal b-jets	-	-		= 0
$E_{\mathrm{T}}^{\mathrm{miss,rel.}}$	> 40	> 100		> 50
other	$m_{\mathrm{T2}} > 90$	-		m_{CT}-veto

Table 2: Signal regions. OS (SS) denotes two opposite-sign (same-sign) signal leptons, of same (SF) or different (DF) flavour. The Z-veto rejects events with m_{ll} within 10 GeV of the Z-mass (91.2 GeV). The m_{CT}-veto rejects events kinematically consistent with $t\bar{t}$. The values quoted for $E_{\mathrm{T}}^{\mathrm{miss,rel}}$ and m_{T2} are in units of GeV.

fixed 190 GeV slepton mass, this product increases from 0.2 to 4.0% as the neutralino mass decreases from 140 to 20 GeV. In the simplified models, for $\tilde{\chi}_1^{\pm}\tilde{\chi}_1^{\mp}$ pair production, the product of acceptance and efficiency ranges between 1 and 7%, increasing towards higher chargino and lower neutralino masses.

In SR-OSjveto a different approach to reducing the backgrounds is taken. The explicit jet veto in SR-OSjveto suppresses the $t\bar{t}$ background. The dominant Z background is suppressed by rejecting events with m_{ll} within 10 GeV of the Z-mass. The final requirement, on $E_{\mathrm{T}}^{\mathrm{miss,rel.}}$, further increases sensitivity to the signals which are associated with much higher $E_{\mathrm{T}}^{\mathrm{miss}}$ than the SM backgrounds. In the simplified models, for $\tilde{\chi}_1^{\pm}\tilde{\chi}_1^{\mp}$ pair production, the product of acceptance and efficiency ranges between 1 and 8%, increasing towards higher chargino and lower neutralino masses.

5.2 Other Weak Gaugino Production

In the production channel and decay $\tilde{\chi}_2^0\tilde{\chi}_i \rightarrow (l^{\pm}l^{\mp}\tilde{\chi}_1^0) + (q\bar{q}'\tilde{\chi}_1^0)$ the resulting OS two lepton final state has significant $E_{\mathrm{T}}^{\mathrm{miss}}$ and at least two signal jets. The region SR-2jets is thus sensitive to these decays. In SR-2jets, top background is reduced using a "top-tag" veto. The top-tagging requirement is imposed through the use of the contransverse mass variable m_{CT} [59]. This observable can be calculated from the four-momenta of the selected signal jets and leptons:

$$m_{\mathrm{CT}}^2(v_1, v_2) = [E_{\mathrm{T}}(v_1) + E_{\mathrm{T}}(v_2)]^2 - [\mathbf{p}_{\mathrm{T}}(v_1) - \mathbf{p}_{\mathrm{T}}(v_2)]^2 , \quad (2)$$

where v_i can be a lepton (l), jet (j) or a lepton-jet combination. Transverse momentum vectors are defined by $\mathbf{p}_{\mathrm{T}}$ and transverse energies E_{T} are defined as $E_{\mathrm{T}} = \sqrt{p_{\mathrm{T}}^2 + m^2}$. The quantities $m_{\mathrm{CT}}(j, j)$, $m_{\mathrm{CT}}(l, l)$ and $m_{\mathrm{CT}}(jl, jl)$ are bounded from above by analytical functions of the top quark and W boson masses. A top-tagged event must have at least two jets with $p_{\mathrm{T}} > 20$ GeV, and the scalar sum of the p_{T} of at least one combination of two signal jets and the two signal leptons in the event must exceed 100 GeV. Furthermore, top-tagged events are required to possess m_{CT} values calculated from combinations of signal jets and leptons consistent with the expected bounds from $t\bar{t}$ events as described in Ref. [60]. Further top rejection is achieved using a b-jet veto. Z backgrounds are reduced using the Z-veto, and sensitivity increased by searching at high-$E_{\mathrm{T}}^{\mathrm{miss,rel.}}$.

In the regions targeting fully leptonic $\tilde{\chi}_2^0\tilde{\chi}_1^{\pm}$ decays (SR-OSjveto and SR-SSjveto), a veto on events containing a signal jet reduces hadronic backgrounds, and high $E_{\mathrm{T}}^{\mathrm{miss,rel.}}$ increases the sensitivity to SUSY decays. The final state leptons can be of either OS or SS. In the absence of significant expected Z background in the SS SR, no Z-veto is applied.

	top	WW	$Z + X$
m_{ll}	Z-veto	Z-veto	Z-window
signal jets	≥ 2	=0	$= 0, \geq 2, \geq 0$
signal b-jets	≥ 1	=0	$\geq 0, = 0, \geq 0$
$E_{\mathrm{T}}^{\mathrm{miss,rel.}}$	$> 100, 50, 40$	70-100	$> 100, 50, 40$
other	-	-	-, m_{CT}-veto, -

Table 3: Requirements for entering each CR for top, WW and $Z + X$ background estimation in the OS SR. These are used to estimate the top background in all OS SR, WW in SR-OSjveto and $Z + X$ in all SF channels of the OS SR. When each OS SR requires differing CR definitions, the conditions are given as a comma separated list (SR-OSjveto, SR-2jets, SR-m_{T2}). The Z-veto is a rejection of events with m_{ll} within 10 GeV of the Z-mass (91.2 GeV), whereas the Z-window defines the reverse. In the WW control region the b-jets considered are those with $p_{\mathrm{T}} > 20$ GeV. The values quoted for $E_{\mathrm{T}}^{\mathrm{miss,rel}}$ are in units of GeV.

6 Background Evaluation

6.1 Backgrounds in SR-m_{T2}

In this note, SR-m_{T2} is used to search for $\tilde{l}^{\pm}$ pair production and provides the best sensitivity to $\tilde{\chi}_1^{\pm}$ pair production. The main backgrounds in this region are: fully-leptonic $t\bar{t}$ and single top, Z/γ^*+jets and dibosons (WW, WZ and ZZ).

Fully-leptonic $t\bar{t}$ is comparable in size to the WW background in all flavour channels. Z/γ^*+jets, WZ and ZZ processes (collectively, $Z+X$) are a small proportion of events in the DF channel, but comparable in size to the WW and $t\bar{t}$ backgrounds in the SF channels. The remainder of the SM background is accounted for by fake lepton backgrounds. The methods used to evaluate these backgrounds in SR-m_{T2} are described in the following sections.

6.1.1 Top

The combined contribution from $t\bar{t}$ and Wt-channel single top events in each channel is evaluated by normalising MC to data in an appropriate CR. Events in the CR (Table 3) must contain at least two signal jets, one of which must be b-tagged, and pass the requirement that $E_{\mathrm{T}}^{\mathrm{miss,rel.}}$ must be greater than 40 GeV. The corresponding CR is dominated by top events. The contamination from non-top events is less than 4%. The number of top events in the SR ($N_{\mathrm{top}}^{\mathrm{SR}}$) is estimated from the number of data events in the CR ($N_{\mathrm{top}}^{\mathrm{CR}}$), after the subtraction of non-top backgrounds, using a transfer factor $\mathcal{T}$:

$$N_{\mathrm{X}}^{\mathrm{SR}} = N_{\mathrm{X}}^{\mathrm{CR}} \times \mathcal{T} \times \mathrm{S}_{\mathcal{T}}. \tag{3}$$

The factor, $\mathcal{T}$, the ratio of top events in the SR to the CR is derived using MC.

$$\mathcal{T} = \left(\frac{N_{\mathrm{X}}^{\mathrm{SR}}}{N_{\mathrm{X}}^{\mathrm{CR}}} \right)_{\mathrm{MC}}. \tag{4}$$

The factor $\mathrm{S}_{\mathcal{T}}$ corrects for possible differences in jet-veto efficiency between data and MC. Good agreement is observed in separate samples of $t\bar{t}$ and Z/γ^*+jets events and so this factor is taken to be equal to 1, with an uncertainty of 6%.

The transfer factor is evaluated before the m_{T2} requirement is applied in the SR. Limited statistics do not allow the factor to be evaluated after this requirement without introducing significant uncertainty (by

design this is the tail of the m_{T2} distribution for $t\bar{t}$). The efficiency of this requirement is then evaluated using MC for a looser selection (which is assumed not to change the m_{T2} shape) and used to obtain the final estimate in SR-m_{T2}. The efficiency of the m_{T2} requirement is found to be ~ 0.02 in each channel for top events with an uncertainty of $\sim 50\%$. The uncertainty is largely dominated by MC statistical uncertainty, generator uncertainties and jet and lepton scales and resolutions.

The evaluated $t\bar{t}$ components in each channel are consistent with pure MC estimates normalised to cross-sections to within 1σ. There is also consistent agreement at this level between data and MC in the CR. Negligible contamination from the SUSY signal models generated, in the region of the expected reach, is predicted.

6.1.2 $Z + X$

The Z/γ^*+jets background in the SF channels is also estimated by normalising MC to data in a suitable CR. This is important in order to handle appropriately possible detector imperfections affecting $E_{\mathrm{T}}^{\mathrm{miss}}$ mis-measurement. This technique also estimates the ZW and ZZ components, providing a combined estimate of the total $Z + X$ background in the SF channels.

In the DF channel the Z/γ^*+jets contribution is significantly smaller and arises mainly from $Z/\gamma^* \rightarrow \tau\tau$ decays. This and the diboson components of the $Z + X$ background in the DF channel are estimated using MC.

The CR (Table 3) used to estimate the $Z+X$ background in the SF channels is defined to be identical to the SR but with the Z-veto reversed. The normalisation is evaluated before the m_{T2} requirement, and the efficiency of the m_{T2} requirement measured separately and applied. The population of data events inside the CR not produced by $Z+X$ processes is estimated using data $e\mu$ events inside the Z-window, correcting for the differences between electron and muon reconstruction efficiencies. This subtraction removes less than 2% of the events in the CR. This procedure also subtracts contributions from $Z/\gamma^* \rightarrow \tau\tau$+jets events which must be estimated using MC simulation. The MC m_{T2} requirement efficiency for $Z + X$ events is taken to be 0.004 (0.003) for e^+e^- ($\mu^+\mu^-$) events with $\sim 50\%$ uncertainty.

The resulting estimates in the SF channels are consistent with MC at the 1σ level. No significant signal contamination is expected for the SUSY model points considered in the region of sensitivity for the searches reported in this note.

6.1.3 WW

The WW background is evaluated using MC normalised to cross-section and luminosity. The predictions from a variety of generators (see Section 3) were compared before application of the m_{T2} requirement (to maximise statistics for comparison), in order to assess the theoretical uncertainty on this estimate. The m_{T2} distribution in data agrees well with that in MC, and the $E_{\mathrm{T}}^{\mathrm{miss,rel.}}$ region under consideration (> 40 GeV) is close to the bulk of the WW sample.

6.1.4 Fake leptons

In this note the term "fake leptons" refers to both misidentified jets and real leptons that arise from decays or conversions. The numbers of fake lepton events are estimated using the "matrix method" [61]. First, fake leptons are identified as those satisfying a loose set of identification requirements corresponding to medium-level identification requirements and no isolation. The real efficiency r is calculated using data as the fraction of these loose leptons passing the signal lepton identification and isolation requirements in events lying within 5 GeV of the Z-mass. The fake efficiency f is calculated separately for misidentified jets or decays and conversions. The fake efficiency for misidentified jets or decays is calculated using MC events with $E_{\mathrm{T}}^{\mathrm{miss,rel.}}$ between 40 and 100 GeV. The fake efficiency for conversions is estimated using

di-muon events in data with m_{ll} within 10 GeV of the Z-mass, $E_{\mathrm{T}}^{\mathrm{miss,rel.}} < 50$ GeV and at least one loose electron with $m_{\mathrm{T}} < 40$ GeV (the conversion candidate). The overall f used is then the weighted (according to the relative proportions of each component present in the SR) average of these two fake efficiencies. Then, in the SR the observed numbers of events in data with two loose leptons, two signal leptons, or one of each are counted. The number of events containing fake leptons in each SR is finally obtained by acting on these observed counts with a 4×4 matrix with terms containing f and r which relates real-real, real-fake, fake-real and fake-fake lepton event counts to tight-tight, tight-loose, loose-tight and loose-loose counts.

6.2 Backgrounds in SR-OSjveto, SR-SSjveto and SR-2jets

The same techniques are used to estimate the backgrounds in each remaining SR, with two exceptions which are detailed in this section. Table 3 details any changes to CR definitions used.

1. Due to the high $E_{\mathrm{T}}^{\mathrm{miss,rel.}}$ requirement (> 100 GeV) in SR-OSjveto, WW is estimated using MC normalised to data in a CR. The CR used for its estimate is defined using the same requirements as the SR but with slightly lower $E_{\mathrm{T}}^{\mathrm{miss,rel.}}$ (for orthogonality with the SR) and an additional b-jet veto to suppress $t\bar{t}$ (Table 3). This CR is subject to a 24% contamination from top events, which is subtracted using MC.

2. In SR-SSjveto, the leptons have the same charge, resulting in a generally different background composition, and the presence of an additional component: "charge-flip". The background components in this region are: fake leptons (estimated using the described matrix method), dibosons (estimated using MC) and charge-flip. Charge-flip background arises when an electron in an event undergoes hard bremsstrahlung with subsequent photon conversion. The probability of an electron undergoing a flip is measured from Z events in data using a likelihood technique [62], and in MC. This probability, evaluated as a function of electron rapidity and p_{T}, is applied to $t\bar{t} \to e^{\pm}l^{\mp}$, Z+jets and diboson MC events to evaluate the number of $e^{\pm}e^{\pm}$ and $e^{\pm}\mu^{\pm}$ events resulting from the charge-flip mechanism. The probability of misidentifying the charge of a muon is negligible. The possible double counting of charge-flip events in the matrix method for SR-SSjveto is not significant.

7 Systematic Uncertainties

In this analysis systematic uncertainties arise on the estimates of the background in the signal regions, as well as on the estimate of the SUSY signal itself. The primary sources of systematic uncertainty are the jet energy scale (JES) calibration, the jet energy resolution (JER) uncertainty [51], theory and MC modelling uncertainties, and uncertainties on the object reconstruction and identification. Additional statistical uncertainties arise from limited numbers of MC and data events in the CR and SR, and a 3.9% luminosity uncertainty [63, 64] for normalising MC to cross-sections.

The JES has been determined from a combination of test beam, simulation and in-situ measurements from 2011 pp collision data. Uncertainties on the lepton identification, momentum/energy scale and resolution are estimated from samples of $Z \to l^+l^-$, $J/\psi \to l^+l^-$ and $W^{\pm} \to l^{\pm}\nu$ decays [65, 66]. The uncertainties on the jet and lepton energies are propagated to $E_{\mathrm{T}}^{\mathrm{miss,rel.}}$; an additional uncertainty on $E_{\mathrm{T}}^{\mathrm{miss}}$ arising from energy deposits not associated to any reconstructed objects is also included. Uncertainties on the b-tagging efficiency are derived from data samples containing muons associated to jets [67] and the method described in Ref. [68]. Included are uncertainties in the mis-tag rate from charm [69], and light flavour tagging [70].

Theory and MC modelling uncertainties are evaluated for $t\bar{t}$ using the prescriptions described in Ref. [71] (choice of generator, and ISR/FSR). For dibosons they are considered by varying the choice of

generator. Theoretical uncertainties on the Z/γ^*+jets background from varying the PDF and renormalisation scales are also included.

When evaluating the fake lepton component in each region the dominant uncertainties arise from variations in the choice of CR, the dependency of the efficiencies on $E_{\mathrm{T}}^{\mathrm{miss,rel.}}$, differences between efficiencies obtained using OS and SS events and uncertainties in the relative normalisations of the different components.

The relative sizes of these sources of systematic uncertainty are detailed in Table 4. In SR-m_{T2} jet and lepton energy scales and resolutions are the most significant uncertainties. In SR-OSjveto and SR-2jets, where $t\bar{t}$ and WW are the most significant SM backgrounds (accounting for approximately 80-85% of the SM contribution), the uncertainties in the MC modelling dominate. In SR-SSjveto, because of the significant fake component, the error on the fake estimate from the sources described becomes the only significant source of uncertainty.

SR-	m_{T2}	OSjveto	2jets	SSjveto
Total statistical	9	4	6	13
Total systematic	19	19	49	35
Jet systematics	9	8	5	3
Lepton systematics	14	1	5	1
b-tagging efficiency	1	1	14	0
MC modelling	7	17	45	4
Fake leptons	5	5	4	35

Table 4: Systematic uncertainties (%) on the background estimates in each SR for all flavours combined. The total statistical uncertainty includes limited MC statistics in the CR and SR. Jet systematics include: JES, JER and $E_{\mathrm{T}}^{\mathrm{miss}}$ cluster and pile-up uncertainties. Lepton systematics include: all lepton scales and resolutions, reconstruction and trigger efficiencies. MC modelling uncertainties include choice of generator, ISR/FSR and modelling of the Z/γ^*+jets line-shape.

In the SUSY mass planes, the theoretical uncertainty on each of the signal cross-sections is included. These arise from considering the cross-section envelope defined using the 68% C.L. ranges of the `CTEQ6.6` and `MSTW 2008 NLO` PDF sets, and independent variations of the factorisation and renormalisation scales (see Section 3). Further uncertainties on the numbers of predicted signal events arise from the various experimental uncertainties.

8 Results and Interpretation

Figures 1 to 3 illustrate data and MC (but with the fake lepton component evaluated using the matrix method) in the various CR. The hashed region illustrates the size of the experimental uncertainties.

Figure 4 illustrates the level of agreement in each SR. For each SR two illustrative model points are also presented.

Table 5 compares the observations in data in each flavour channel and in each SR with the evaluated background contributions. Good agreement is observed across all channels and in each SR. The absence of evidence for SUSY weak production allows limits to be set on the visible cross-section for non-SM physics in each SR, $\sigma_{\mathrm{vis}} = \sigma \times \varepsilon \times A$, for which this analysis has acceptance A and efficiency ε. These are calculated using the modified frequentist $\mathrm{CL_s}$ prescription [72] by comparing the number of observed events in data with the SM expectation using the profile likelihood ratio as test statistic. All systematic uncertainties and their correlations are taken into account via nuisance parameters.

The direct slepton pair production 95% exclusion region is shown in Figure 5 (a) in the neutralino-slepton mass plane, using the results of SR-m_{T2} in the SF channel. Shown are the 95% $\mathrm{CL_s}$ expected

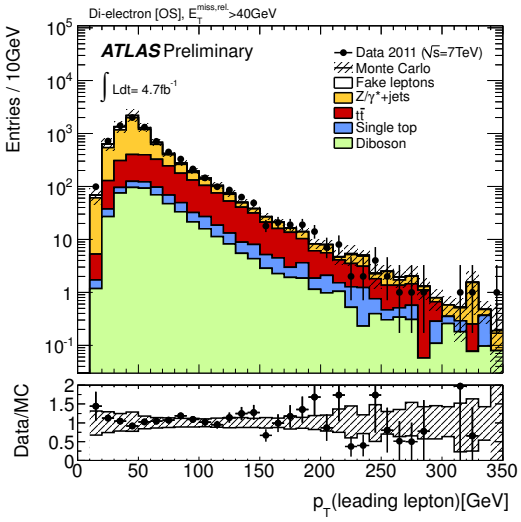

(a)

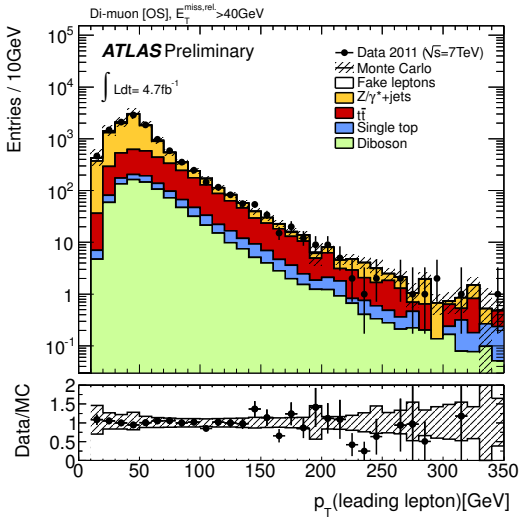

(b)

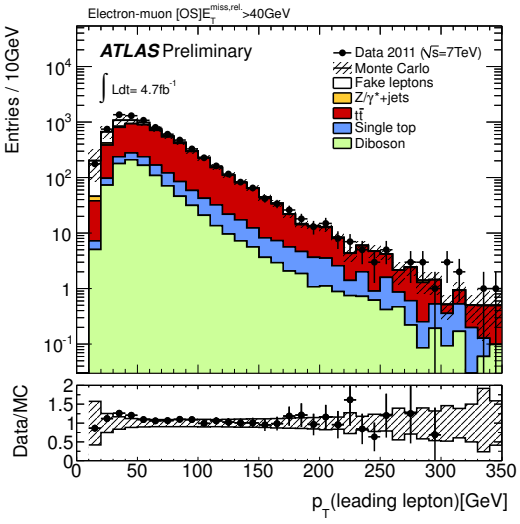

(c)

Figure 1: The leading lepton p_{T} distributions in the e^+e^- (a), $\mu^+\mu^-$ (b) and $e^\pm\mu^\mp$ (c) channels after the application of the $E_{\mathrm{T}}^{\mathrm{miss,rel.}} > 40$ GeV cut. The hatched bands indicate the experimental uncertainties on the background expectations. All components are from MC except for that which is labelled "Fake leptons". The bottom panels show the ratio of the data to the expected background (points) and the systematic uncertainty on the background (shaded area).

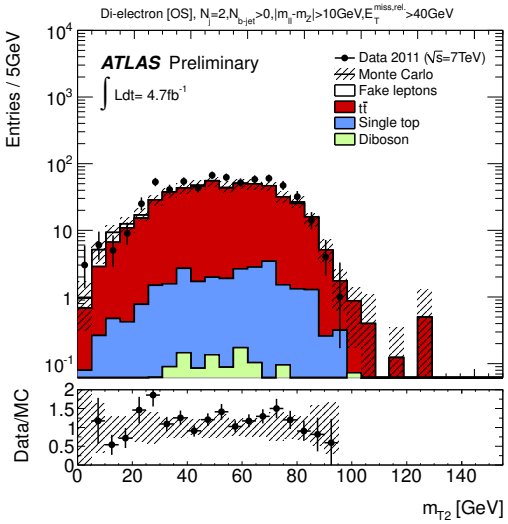

(a)

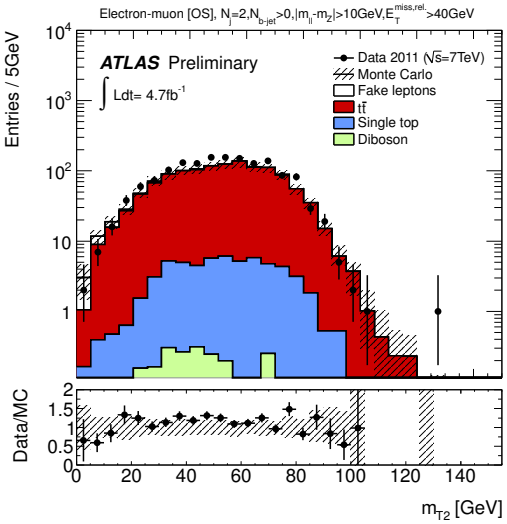

(b)

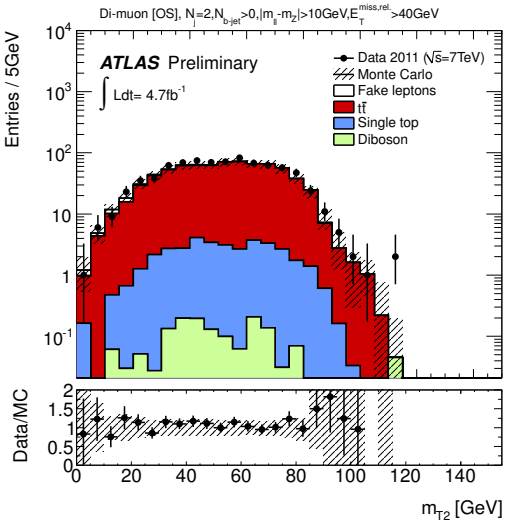

(c)

Figure 2: The m_{T2} distribution in the e^+e^- (a), $e^\pm\mu^\mp$ (b) and $\mu^+\mu^-$ (c) channels top control region for SR-m_{T2}. The hatched bands indicate the experimental uncertainties on the background expectations. All components are from MC except for that which is labelled "Fake leptons". The bottom panels show the ratio of the data to the expected background (points) and the systematic uncertainty on the background (shaded area).

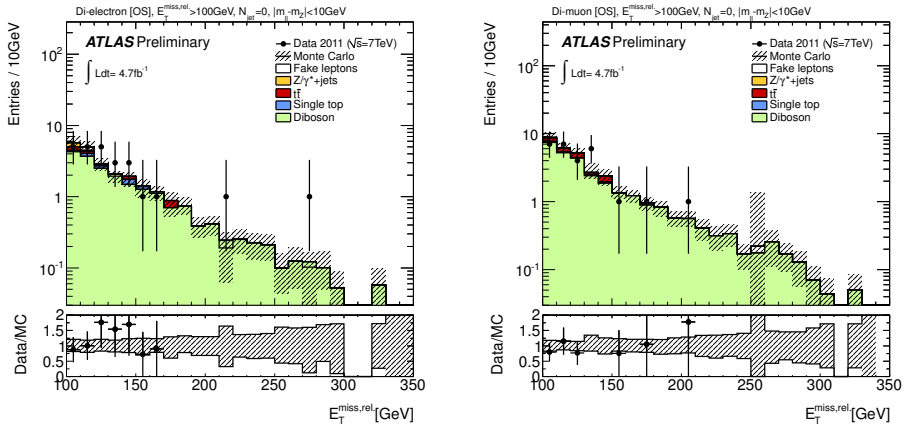

(a)

(b)

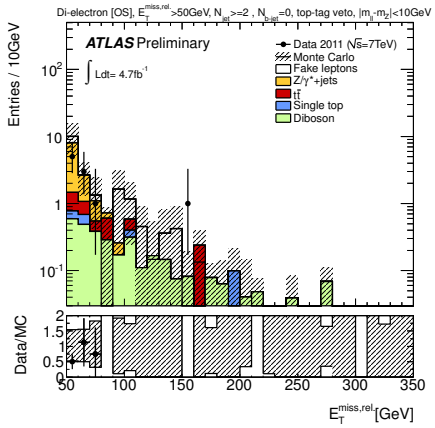

(c)

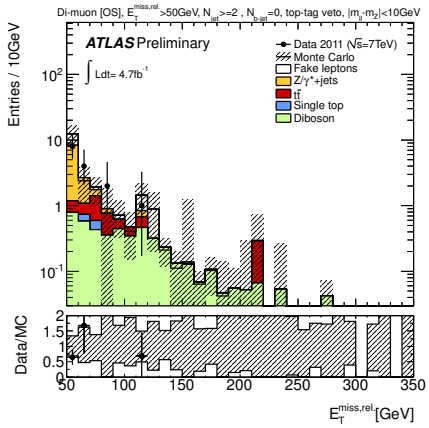

(d)

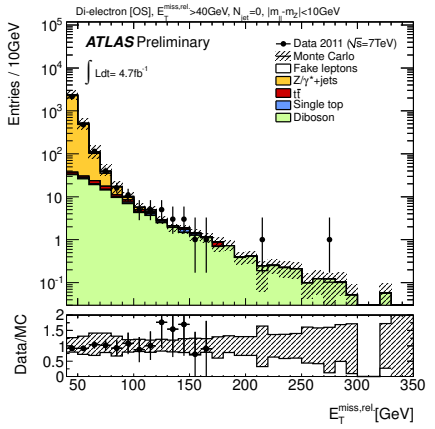

(e)

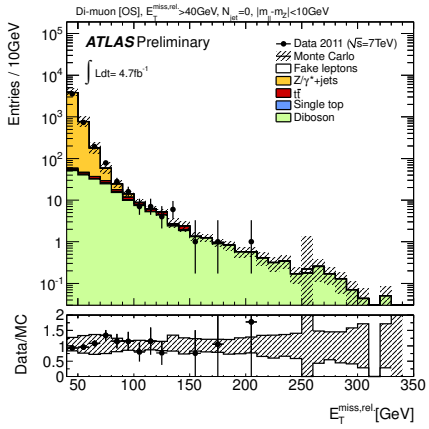

(f)

Figure 3: The $E_{\mathrm{T}}^{\mathrm{miss}}$ distributions for e^+e^- and $\mu^+\mu^-$ events in each Z CR: for SR-jveto (a) and (b), SR-2jets (c) and (d), and SR-m_{T2} (e) and (f). The hatched bands indicate the experimental uncertainties on the background expectations. All components are from MC except for that which is labelled "Fake leptons". The bottom panels show the ratio of the data to the expected background (points) and the systematic uncertainty on the background (shaded area).

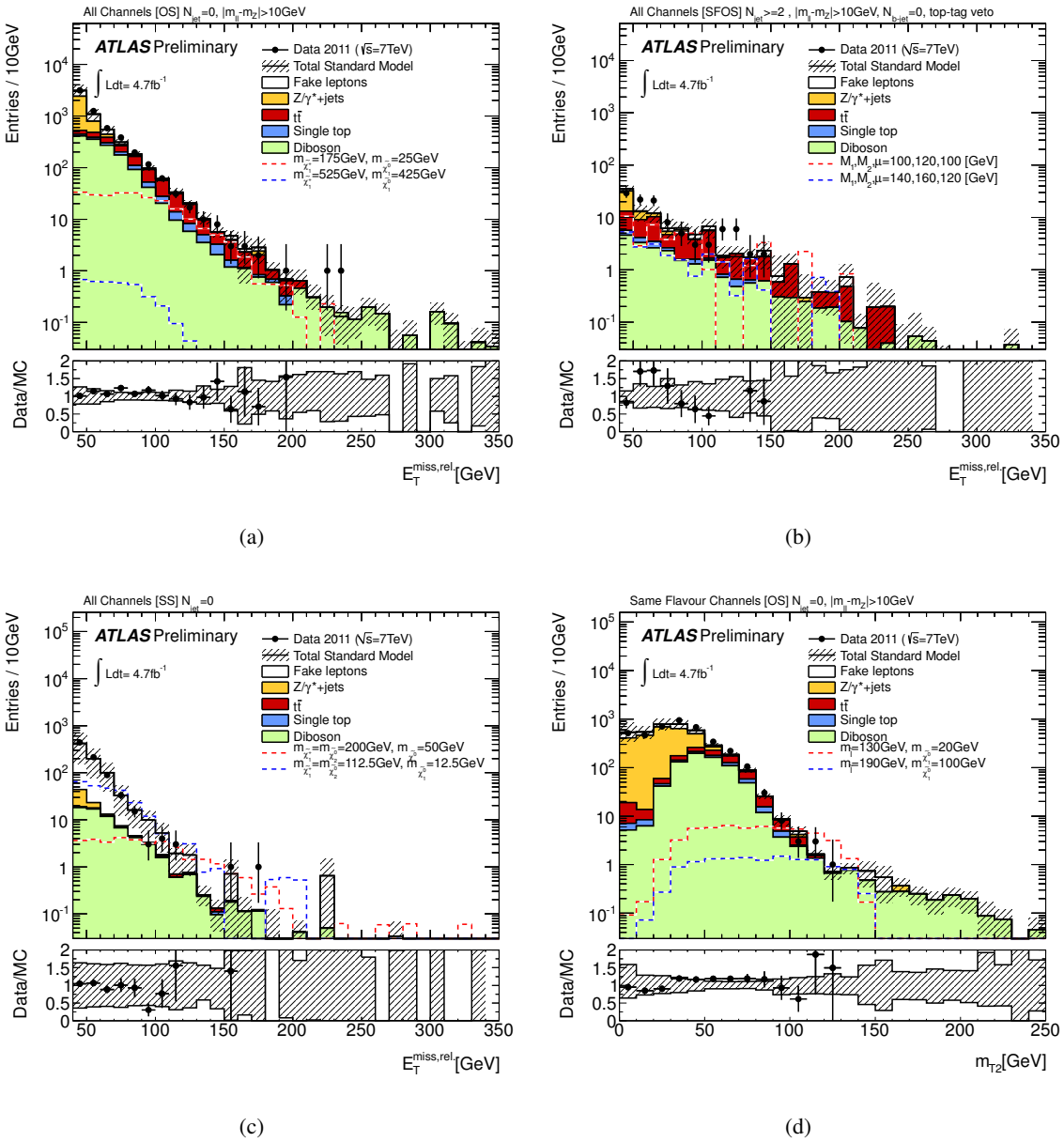

Figure 4: The $E_{\mathrm{T}}^{\mathrm{miss,rel.}}$ distributions for SR-OSjveto (a), SR-2jets (b) and SR-SSjveto (c) in the high-$E_{\mathrm{T}}^{\mathrm{miss,rel.}}$ (> 40 GeV) region, and m_{T2} in SR-mT2 (d), prior to the application of the m_{T2} requirement. In (d) only the SF channels are shown. The hatched bands indicate the experimental uncertainties on the background expectations. All components are from MC except for that which is labelled "Fake leptons". The bottom panels show the ratio of the data to the expected background (points) and the systematic uncertainty on the background (shaded area). In each figure two signal points are illustrated. In (d) two models of direct slepton pair production are illustrated, with $(\tilde{l},\tilde{\chi}_1^0)$ masses of (130,20) and (190,100) GeV. In (a) the two points illustrated are for $\tilde{\chi}_1^{\pm}\tilde{\chi}_1^{\mp}$ production in the simplified model with $(\tilde{\chi}_1^{\pm},\tilde{\chi}_1^0)$ masses of (175,25) and (525,425) GeV. In (c) the simplified model points illustrated have $(\tilde{\chi}_1^{\pm},\tilde{\chi}_1^0)$ masses of (200,50) and (112.5,12.5) GeV. In (b) two pMSSM model points with masses (M_1, M_2, M_μ) of (100,120,100) and (140,160,120) GeV are illustrated.

SR-m_{T2}					
	e^+e^-	$e^\pm\mu^\mp$	$\mu^+\mu^-$	all	SF
Z+X	3.2 ± 1.1 ± 1.7	0.3 ± 0.1 ± 0.2	3.6 ± 1.3 ± 1.7	7.1 ± 1.7 ± 2.1	6.8 ± 1.7 ± 2.1
WW	2.3 ± 0.3 ± 0.4	4.8 ± 0.4 ± 0.7	3.5 ± 0.3 ± 0.5	10.6 ± 0.6 ± 1.5	5.8 ± 0.4 ± 0.9
$t\bar{t}$, single top	2.6 ± 1.2 ± 1.3	6.2 ± 1.6 ± 2.9	4.1 ± 1.3 ± 1.6	12.9 ± 2.4 ± 4.6	6.8 ± 1.8 ± 2.3
Fake leptons	1.0 ± 0.6 ± 0.6	1.1 ± 0.6 ± 0.8	−0.02 ± 0.01 ± 0.05	2.2 ± 0.9 ± 1.4	1.0 ± 0.6 ± 0.6
Total	9.2 ± 1.8 ± 2.5	12.4 ± 1.7 ± 3.1	11.2 ± 1.9 ± 3.0	32.8 ± 3.2 ± 6.3	20.4 ± 2.6 ± 3.9
Data	7	9	8	24	15
$\sigma_{vis}^{obs(exp)}$ (fb)	1.6 (1.9)	1.7 (2.2)	1.7 (2.1)	2.6 (3.8)	2.0 (2.7)

SR-OSjveto				
	e^+e^-	$e^\pm\mu^\mp$	$\mu^+\mu^-$	all
Z+X	4.5 ± 1.2 ± 1.2	3.0 ± 0.9 ± 0.5	4.7 ± 1.1 ± 1.2	12.2 ± 1.8 ± 1.8
WW	8.8 ± 1.8 ± 4.4	20.9 ± 2.6 ± 6.2	13.3 ± 1.9 ± 3.5	43.0 ± 3.7 ± 12.2
$t\bar{t}$, single top	21.1 ± 2.3 ± 4.2	47.7 ± 3.4 ± 20.5	27.5 ± 2.5 ± 9.0	96.2 ± 4.8 ± 29.5
Fake leptons	2.9 ± 1.2 ± 1.2	6.9 ± 1.8 ± 2.6	0.4 ± 0.6 ± 0.3	10.3 ± 2.2 ± 4.1
Total	37.2 ± 3.3 ± 6.4	78.5 ± 4.7 ± 20.9	45.9 ± 3.4 ± 9.4	161.7 ± 6.7 ± 30.8
Data	33	66	40	139
$\sigma_{vis}^{obs(exp)}$ (fb)	3.5 (4.0)	8.1 (9.6)	4.3 (5.1)	11.4 (14.1)

SR-2jets				
	e^+e^-	$e^\pm\mu^\mp$	$\mu^+\mu^-$	SF
Z+X	3.8 ± 1.3 ± 2.7	—	5.8 ± 1.6 ± 3.9	9.6 ± 2.0 ± 5.1
WW	6.4 ± 0.5 ± 4.3	—	8.4 ± 0.6 ± 5.7	14.8 ± 0.7 ± 9.9
$t\bar{t}$, single top	14.8 ± 1.9 ± 9.2	—	22.1 ± 2.1 ± 20.7	36.9 ± 2.9 ± 29.6
Fake leptons	2.5 ± 1.2 ± 1.5	—	1.7 ± 1.3 ± 0.8	4.2 ± 1.8 ± 2.3
Total	27.5 ± 2.6 ± 10.6	—	37.9 ± 3.0 ± 21.0	65.5 ± 4.0 ± 31.8
Data	39	—	39	78
$\sigma_{vis}^{obs(exp)}$ (fb)	7.1 (5.1)	—	9.7 (9.6)	15.6 (13.9)

SR-SSjveto				
	e^+e^-	$e^\pm\mu^\pm$	$\mu^+\mu^-$	all
Charge flip	0.49 ± 0.03 ± 0.17	0.34 ± 0.02 ± 0.11	—	0.83 ± 0.04 ± 0.18
Dibosons	0.62 ± 0.13 ± 0.18	1.93 ± 0.23 ± 0.36	0.94 ± 0.16 ± 0.26	3.50 ± 0.31 ± 0.54
Fake leptons	3.2 ± 0.9 ± 1.7	2.9 ± 0.9 ± 1.9	0.6 ± 0.6 ± 0.3	6.6 ± 1.4 ± 3.8
Total	4.3 ± 0.9 ± 1.7	5.1 ± 1.0 ± 1.9	1.5 ± 0.6 ± 0.4	11.0 ± 1.5 ± 3.9
Data	1	5	3	9
$\sigma_{vis}^{obs(exp)}$ (fb)	0.8 (1.2)	1.5 (1.5)	1.3 (0.8)	2.0 (2.3)

Table 5: Evaluated SM backgrounds in each SR separated by flavour (ee, $e\mu$, $\mu\mu$) and combined in an "all" channel. In SR-m_{T2} the evaluated background components in the SF channel are quoted separately as the $e\mu$ channel is not appropriate for a direct slepton search. The second quoted error is the total systematic uncertainty whereas the first is the statistical uncertainty arising from limited numbers of MC events. The effect of limited data events in the CR is included in the systematic uncertainty. In all OS SR and channels the component Z+X includes the contributions from Z/γ^*+jets, WZ and ZZ events. All statistical uncertainties are added in quadrature whereas the systematic uncertainties are obtained after taking full account of all correlations between sources, backgrounds and channels. Quoted also are the observed (expected) 95% confidence limits on the visible cross-section for non-SM events in each SR, $\sigma_{vis}^{obs(exp)}$.

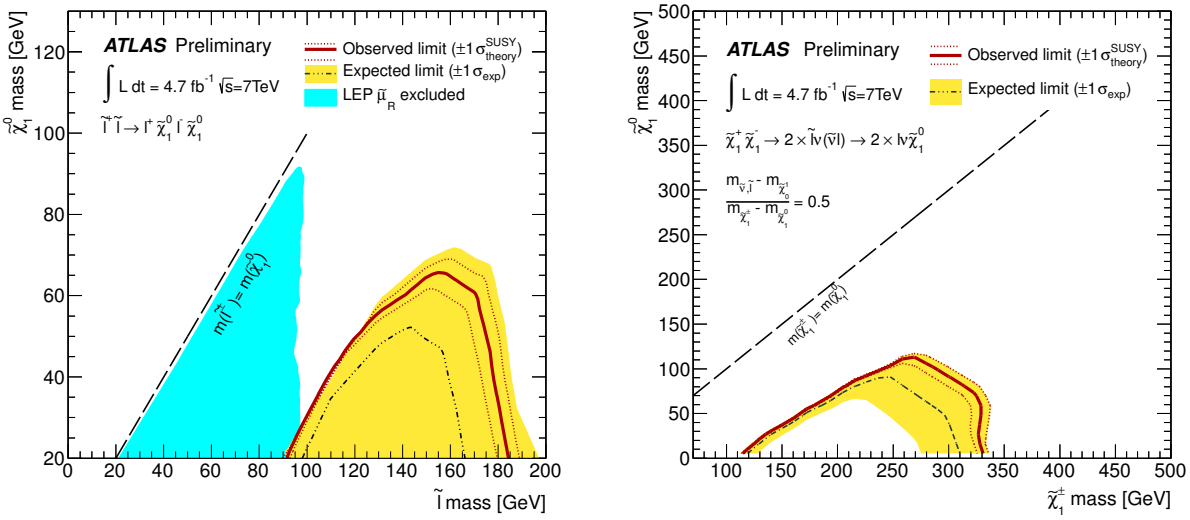

(a) (b)

Figure 5: 95% exclusion limits for $\tilde{l}^{\pm}$ pair production in the $m_{\tilde{l}} - m_{\tilde{\chi}_1^0}$ mass plane of the direct slepton pMSSM (a) and $\tilde{\chi}_1^{\pm}\tilde{\chi}_1^{\mp}$ pair production in the simplified model (b). The dashed black and solid red lines show the 95% CL_s expected and observed limits, respectively, including all uncertainties except for the theoretical signal cross-section uncertainty (PDF and scale). The yellow band around the expected limit shows the $\pm 1\sigma$ result where all uncertainties, except those on the signal cross-sections, are considered. The $\pm 1\sigma$ lines around the observed limit represent the results obtained when moving the nominal signal cross-section up or down by the $\pm 1\sigma$ theoretical uncertainty. Illustrated also in (a) is the LEP limit [25] on the mass of the right-handed smuon, $\tilde{\mu}_R$.

(dashed black) and observed limits (solid red) obtained by including all uncertainties except the theoretical signal cross-section uncertainty. The yellow band indicates the impact of the experimental uncertainties on the expected limits whereas the dashed red lines around the observed limit show the changes in the observed limit as the nominal signal cross-sections are scaled up and down by the 1σ theoretical uncertainties. A common value for left-handed electron and left-handed smuon mass between 90 and 185 GeV is excluded when the lightest neutralino has a mass of 20 GeV. The sensitivity decreases as the the value of $m_{\tilde{l}} - m_{\tilde{\chi}_1^0}$ decreases and gives rise to end-points in the m_{T2} distribution at lower mass, nearer to the end-points of the SM backgrounds. For a 60 GeV neutralino only sleptons with masses between 150 and 170 GeV are excluded.

The direct $\tilde{\chi}_1^{\pm}$ pair production limits are set for the simplified model, in the scenario of wino-like charginos decaying into the lightest neutralino via an intermediate on-shell charged slepton. The best limits are obtained by using for each signal point the SR which provides the best expected p-value. The resulting limit for $\tilde{\chi}_1^{\pm}\tilde{\chi}_1^{\mp}$ production is illustrated in Figure 5 (b). Chargino masses between 110 and 330 GeV are excluded at 95% confidence level for a 10 GeV neutralino. The best sensitivity is provided by SR-m_{T2}. Earlier gaugino searches at the Tevatron and the LHC [26–29] focused on $\tilde{\chi}_1^{\pm}\tilde{\chi}_2^0$ associated production. The present result provides a new mass limit on $\tilde{\chi}_1^{\pm}$ independently of the mass of the $\tilde{\chi}_2^0$. In Figure 6 limits on $\tilde{\chi}_1^{\pm}\tilde{\chi}_1^{\mp}$ and $\tilde{\chi}_1^{\pm}\tilde{\chi}_2^0$ pair production are shown side by side, with details of the SR used to place the exclusions.

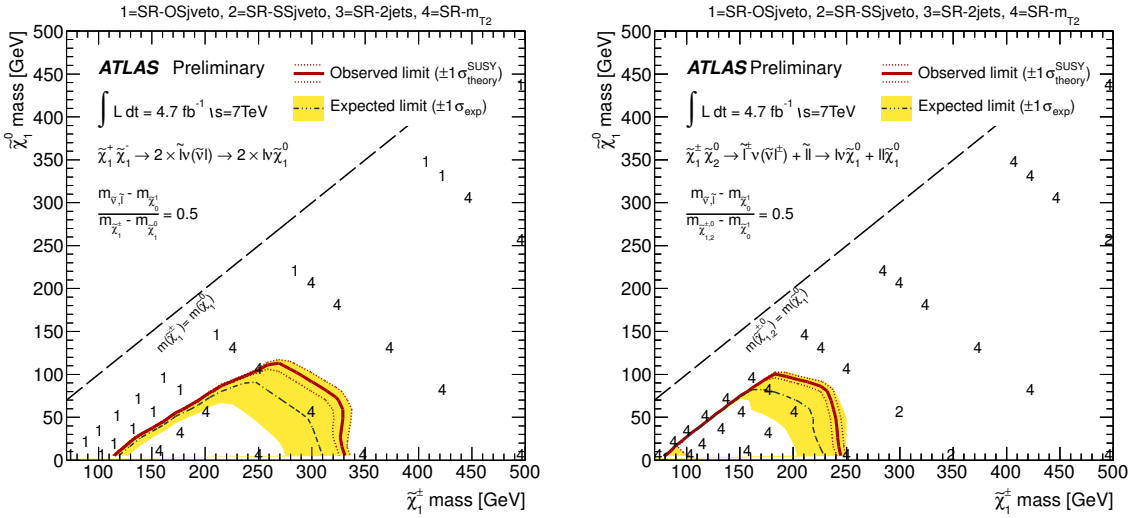

Figure 6: 95% exclusion limits for $\tilde{\chi}_1^{\pm}\tilde{\chi}_1^{\mp}$ and $\tilde{\chi}_1^{\pm}\tilde{\chi}_2^0$ pair production in the simplified model. The overlaid numbers indicate which SR provided the best sensitivity. The dashed black and solid red lines show the 95% $\mathrm{CL_s}$ expected and observed limits, respectively, including all uncertainties except for the theoretical signal cross-section uncertainty (PDF and scale). The yellow band around the expected limit shows the $\pm 1\sigma$ result where all uncertainties, except those on the signal cross-sections, are considered. The $\pm 1\sigma$ lines around the observed limit represent the results obtained when moving the nominal signal cross-section up or down by the $\pm 1\sigma$ theoretical uncertainty.

The model independent limits in Table 5, provide additional constraints on the other gaugino production channels discussed previously in this note. In particular, SR-2jets provides sensitivity to models where one gaugino produced in association with $\tilde{\chi}_2^0$ decays hadronically. The best sensitivity to models where final states containing ≥ 3 leptons dominate would come from a statistical combination of the results set in SR-2jets, SR-OSjveto and SR-SSjveto, and results of searches for three or more leptons [29].

9 Summary

This note has presented a dedicated search for $\tilde{l}^{\pm}$ and $\tilde{\chi}_1^{\pm}$ pair production in final states with two leptons and $E_{\mathrm{T}}^{\mathrm{miss}}$. In scenarios where sleptons decay directly into the lightest neutralino and a charged lepton, left-handed slepton masses between 90 and 185 GeV for a 20 GeV neutralino are excluded at 95% confidence. In the scenario of chargino pair production, with wino-like charginos decaying into the lightest neutralino via an intermediate on-shell charged slepton, chargino masses between 110 and 330 GeV are excluded at 95% confidence for a neutralino of 10 GeV. Signal regions targeting several other gaugino production and decay modes into two-lepton final states have also been used to set limits on the visible cross section.

References

[1] H. Miyazawa Prog. Theor. Phys. **36 (6)** (1966) 1266–1276.

[2] P. Ramond Phys. Rev. **D3** (1971) 2415–2418.

[3] Y. A. Golfand et al. JETP Lett. **13** (1971) 323–326. [Pisma Zh.Eksp.Teor.Fiz.13:452-455,1971].

[4] A. Neveu and J. H. Schwarz Nucl. Phys. **B31** (1971) 86–112.

[5] A. Neveu and J. H. Schwarz Phys. Rev. **D4** (1971) 1109–1111.

[6] J. Gervais and B. Sakita Nucl. Phys. **B34** (1971) 632–639.

[7] D. V. Volkov and V. P. Akulov Phys. Lett. **B46** (1973) 109–110.

[8] J. Wess and B. Zumino Phys. Lett. **B49** (1974) 52.

[9] J. Wess and B. Zumino Nucl. Phys. **B70** (1974) 39–50.

[10] S. Weinberg Phys. Rev. **D13** (1976) 974–996.

[11] E. Gildener Phys. Rev. **D14** (1976) 1667.

[12] S. Weinberg Phys. Rev. **D19** (1979) 1277–1280.

[13] L. Susskind Phys. Rev. **D20** (1979) 2619–2625.

[14] P. Fayet Phys. Lett. **B64** (1976) 159.

[15] P. Fayet Phys. Lett. **B69** (1977) 489.

[16] G. R. Farrar and P. Fayet Phys. Lett. **B76** (1978) 575–579.

[17] P. Fayet Phys. Lett. **B84** (1979) 416.

[18] S. Dimopoulos and H. Georgi Nucl. Phys. **B193** (1981) 150.

[19] A. Djouadi, J.-L. Kneur, and G. Moultaka Comput.Phys.Commun. **176** (2007) 426–455, arXiv:hep-ph/0211331 [hep-ph].

[20] K. L. Chan, U. Chattopadhyay, and P. Nath Phys.Rev. **D58** (1998) 096004, arXiv:hep-ph/9710473 [hep-ph].

[21] M. Dine and A.E. Nelson Phys. Rev. **D48** (1993) 1277; M. Dine, A.E. Nelson, and Y. Shirman Phys. Rev. **D51** (1995) 1362; M. Dine et al. Phys. Rev. **D53** (1996) 2658; G.F. Giudice and R. Rattazzi Phys. Reports 322 419 (1999).

[22] L. Randall and R. Sundrum Nucl. Phys. **B557** (1999) 79-118; G. F. Giudice, M. A. Luty, H. Murayama, R. Rattazzi JHEP 9812, 027 (1998).

[23] G. Belanger, F.Boudjema, A.Cottrant, A. Pukhov, A. Semenov Nucl. Phys. **B706** (2005) 411-454; S. F. King, J. P. Roberts, D. P. Roy JHEP 0710, 106 (2007).

[24] H. Baer et al. Phys. Rev. **D49** (1994) 7.

[25] LEP SUSY Working Group (ALEPH, DELPHI, L3, OPAL), Notes LEPSUSYWG/01-03.1 and 04-01.1, http://lepsusy.web.cern.ch/lepsusy/Welcome.html.

[26] CDF Collaboration Phys. Rev. Lett. **101** (Dec, 2008) 251801.

[27] D0 Collaboration Phys.Lett. **B680** (2009) 34–43, arXiv:0901.0646 [hep-ex].

[28] ATLAS Collaboration Phys.Lett. **B709** (2012) 137–157, arXiv:1110.6189 [hep-ex].

[29] ATLAS Collaboration Phys.Rev.Lett. (2012) , arXiv:1204.5638 [hep-ex].

[30] CMS Collaboration CMS Physics Analysis Summary CMS-PAS-SUS-11-016 (2011).

[31] ATLAS Collaboration JINST **3** (2008) S08003.

[32] S. Frixione, P. Nason, and C. Oleari JHEP **11** (2007) 070.

[33] M. L. Mangano, M. Moretti, F. Piccinini, R. Pittau, and A. D. Polosa JHEP **07** (2003) 001, arXiv:hep-ph/0206293.

[34] T. Gleisberg et al. JHEP **02** (2009) 007.

[35] G. Corcella et al. JHEP **01** (2001) 010, arXiv:hep-ph/0011363.

[36] J. Butterworth, J. Forshaw, and M. Seymour Z. Phys. **C72** (1996) 637–646, hep-ph/9601371.

[37] J. M. Campbell and R. K. Ellis Phys.Rev. **D60** (1999) 113006, arXiv:hep-ph/9905386 [hep-ph].

[38] J. M. Campbell, R. K. Ellis, and C. Williams JHEP **1107** (2011) 018, arXiv:1105.0020 [hep-ph].

[39] M. Aliev, H. Lacker, U. Langenfeld, S. Moch, P. Uwer, et al. Comput.Phys.Commun. **182** (2011) 1034–1046, arXiv:1007.1327 [hep-ph].

[40] R. Gavin, Y. Li, F. Petriello, and S. Quackenbush arXiv:1011.3540 [hep-ph].

[41] S. Frixione and B. R. Webber JHEP **06** (2002) 029; S. Frixione, P. Nason and B. R. Webber JHEP **08** (2003) 007; S. Frixione, E. Laenen and P. Motylinski JHEP **03** (2006) 092.

[42] B. P. Kersevan and E. Richter-Was arXiv:hep-ph/0405247 [hep-ph].

[43] ATLAS Collaboration Eur. Phys. J. **C72** (2012) 2043, arXiv:1203.5015 [hep-ex].

[44] S. AbdusSalam, B. Allanach, H. Dreiner, J. Ellis, U. Ellwanger, et al. Eur.Phys.J. **C71** (2011) 1835, arXiv:1109.3859 [hep-ph].

[45] M. Bahr et al. Eur. Phys. J. **C58** (2008) 639–707, arXiv:0803.0883 [hep-ph].

[46] W. Beenakker, R. Hopker, M. Spira, and P. Zerwas Nucl.Phys. **B492** (1997) 51–103, arXiv:hep-ph/9610490 [hep-ph].

[47] M. Kramer, A. Kulesza, R. van der Leeuw, M. Mangano, S. Padhi, et al. arXiv:1206.2892 [hep-ph].

[48] S. Agostinelli Nucl. Instrum. Meth. **A506** (2003) 250–303.

[49] ATLAS Collaboration European Physical Journal C **70** (Dec., 2010) 823–874, arXiv:1005.4568 [physics.ins-det].

[50] M. Cacciari, G. P. Salam, and G. Soyez JHEP **04** (2008) 063, arXiv:0802.1189 [hep-ph].

[51] ATLAS Collaboration arXiv:1112.6426 [hep-ex].

[52] ATLAS Collaboration JHEP **1012** (2010) 060, arXiv:1010.2130 [hep-ex].

[53] ATLAS Collaboration ATLAS-CONF-2011-015 https://cdsweb.cern.ch/record/1334877 (2011).

[54] ATLAS Collaboration arXiv:1205.2531 [hep-ex].

[55] ATLAS Collaboration ATLAS-CONF-2011-102 https://cdsweb.cern.ch/record/1369219 (2011).

[56] A. Barr, C. Lester, and P. Stephens J.Phys.G **G29** (2003) 2343–2363, arXiv:hep-ph/0304226 [hep-ph].

[57] C. Lester and D. Summers Phys.Lett. **B463** (1999) 99–103, arXiv:hep-ph/9906349 [hep-ph].

[58] ATLAS Collaboration arXiv:0901.0512 [hep-ex].

[59] D. Tovey JHEP **0804** (2008) 034.

[60] G. Polesello and D. Tovey JHEP **1003** (2010) 030.

[61] ATLAS Collaboration Eur. Phys. J. **C71** (2011) 1577, arXiv:1012.1792 [hep-ex].

[62] ATLAS Collaboration JHEP **1204** (2012) 069, arXiv:1202.5520 [hep-ex].

[63] ATLAS Collaboration Eur.Phys.J. **C71** (2011) 1630, arXiv:1101.2185 [hep-ex].

[64] ATLAS Collaboration ATLAS-CONF-2011-116 https://cdsweb.cern.ch/record/1376384 (2011).

[65] ATLAS Collaboration ATLAS-CONF-2011-063 https://cdsweb.cern.ch/record/1345743 (2011).

[66] ATLAS Collaboration ATLAS-CONF-2011-021 https://cdsweb.cern.ch/record/1336750 (2011).

[67] ATLAS Collaboration ATLAS-CONF-2011-102 https://cdsweb.cern.ch/record/1369219 (2011).

[68] ATLAS Collaboration ATLAS-CONF-2011-143 https://cdsweb.cern.ch/record/1386703 (2011).

[69] ATLAS Collaboration ATLAS-CONF-2012-039 https://cdsweb.cern.ch/record/1435193 (2012).

[70] ATLAS Collaboration ATLAS-CONF-2012-040 https://cdsweb.cern.ch/record/1435194 (2012).

[71] ATLAS Collaboration Phys.Lett. **B707** (2012) 459–477, arXiv:1108.3699 [hep-ex].

[72] A. L. Read J.Phys.G **G28** (2002) 2693–2704.